Received: 28 December 2023 | Revised: 9 August 2024 | Accepted: 23 August 2024

DOI: 10.1002/cnm.3867

BASIC RESEARCH

WILEY

Uncertainty quantification of the pressure waveform using a Windkessel model

Joaquín Flores-Gerónimo[1] | **Alireza Keramat**[1] | **Jordi Alastruey**[2] | **Yuanting Zhang**[3]

[1]Department of Civil and Environmental Engineering, The Hong Kong Polytechnic University, Hung Hom, Hong Kong

[2]Department of Biomedical Engineering, School of Biomedical Engineering and Imaging Sciences, King's College London, London, UK

[3]Department of Electronic Engineering, The Chinese University of Hong Kong, Sha Tin, Hong Kong

Correspondence
Alireza Keramat and Joaquín Flores-Gerónimo, Department of Civil and Environmental Engineering, The Hong Kong Polytechnic University, Hung Hom, Hong Kong.
Email: alireza.keramat@polyu.edu.hk and joaquin.flores.iq@gmail.com

Funding information
Hong Kong Center for Cerebro-Cardiovascular Health Engineering; InnoHK; Hong Kong Polytechnic University

Abstract

The Windkessel (WK) model is a simplified mathematical model used to represent the systemic arterial circulation. While the WK model is useful for studying blood flow dynamics, it suffers from inaccuracies or uncertainties that should be considered when using it to make physiological predictions. This paper aims to develop an efficient and easy-to-implement uncertainty quantification method based on a local gradient-based formulation to quantify the uncertainty of the pressure waveform resulting from aleatory uncertainties of the WK parameters and flow waveform. The proposed methodology, tested against Monte Carlo simulations, demonstrates good agreement in estimating blood pressure uncertainties due to uncertain Windkessel parameters, but less agreement considering uncertain blood-flow waveforms. To illustrate our methodology's applicability, we assessed the aortic pressure uncertainty generated by Windkessel parameters-sets from an available in silico database representing healthy adults. The results from the proposed formulation align qualitatively with those in the database and in vivo data. Furthermore, we investigated how changes in the uncertainty of the Windkessel parameters affect the uncertainty of systolic, diastolic, and pulse pressures. We found that peripheral resistance uncertainty produces the most significant change in the systolic and diastolic blood pressure uncertainties. On the other hand, compliance uncertainty considerably modifies the pulse pressure standard deviation. The presented expansion-based method is a tool for efficiently propagating the Windkessel parameters' uncertainty to the pressure waveform. The Windkessel model's clinical use depends on the reliability of the pressure in the presence of input uncertainties, which can be efficiently investigated with the proposed methodology. For instance, in wearable technology that uses sensor data and the Windkessel model to estimate systolic and diastolic blood pressures, it is important to check the confidence level in these calculations to ensure that the pressures accurately reflect the patient's cardiovascular condition.

KEYWORDS

direct differentiation method, hemodynamics, sensitivity analysis, uncertainty quantification, Windkessel model

1 | INTRODUCTION

The Windkessel (WK) model is a simplified mathematical model often used to represent the systemic arterial circulation of blood in the human body. This model assumes that the circulatory system can be lumped into a simple dynamic model that relates arterial pressure and flow variations.[1] The model is governed by an ODE with a few parameters describing global properties of the systemic arterial network.[2] Several studies[3–6] have provided evidence for the utility and accuracy of the WK model in simulating blood flow dynamics in the arterial system. Moreover, in the context of integrating data from diverse modalities for clinical decision-making, a parsimonious model grounded in physiology would be preferable due to its efficiency and ease of use.[7] For instance, pulse control is a method to continuously estimate the cardiac output (CO). This method combines the Windkessel model with blood pressure measurements. Constant CO monitoring is relevant for making clinical decisions when managing critically ill patients.[8]

Prior to launching into further technical issues of the WK model, we should clarify its valuable contribution as a simple but acceptable model to be applied in the preventive cardiovascular healthcare. Specifically in predicting the systolic blood pressure (SBP) and diastolic blood pressure (DBP) from wearables, the collected sensor data—for example, from photoplethysmography (PPG)—can be used to estimate some parameters of the WK model (e.g., impedance), while others are set as known quantities calibrated through other standard cuff-based elaborate methods. With this, the WK model enables to estimate the pressure waveform, including SBP and DBP. Several studies from the literature discuss how the WK model can be used to predict blood pressure using wearable sensors. Among which, Wu et al.[9] have recently proposed a camera-based approach for blood pressure estimation via the WK Model. While such an estimation may suffer from several types of uncertainties, it still is of great value in cardiovascular health as it provides real-time monitoring, early detection of abnormalities, and promotes active lifestyle choices for preventive care. That is also the reason behind the success and market reception of wearables nowadays.

While the WK model is useful for studying blood flow dynamics, it suffers from inaccuracies or uncertainties that should be considered when using it to make physiological predictions. In system identification context, the uncertainties are divided into aleatoric and epistemic uncertainties.[10] Aleatoric uncertainty refers to the inherent randomness or unpredictability in a system, that is, Windkessel parameters herein. Whereas epistemic uncertainty deals with limitations in our assumptions in cardiovascular modeling. The WK model's primary aleatory uncertainty source is its parameters, including compliance, resistance, and impedance.[11] These parameters can significantly vary based on patients' physiology and health status, leading to challenges in accurately estimating them.[5,12] In addition, the approach to evaluating these parameters is prone to measurement errors and variability; for instance, when using Doppler ultrasound to measure the blood flow waveform, inaccuracies may occur due to errors in the measurement of the vessel's cross-sectional area or angle approach.[13] Additional sources of uncertainty (both aleatory and epistemic) in the WK model are the assumptions made about the arterial system's geometry and topology.[14] The model assumes that the arterial system is zero-dimensional, which is a considerable simplification since the arterial network has branching and changing diameters. The model also assumes a uniform flow and pressure distribution throughout the arterial system, which does not hold since the shape of the pulse waves changes as they travel from the heart to the periphery.[1] Furthermore, the WK model does not account for important physiological phenomena like wave reflections and wall viscoelasticity.[1] These phenomena can significantly affect blood flow dynamics, especially in older patients or those with arterial stiffness. Acknowledging these uncertainties of the WK parameters and considering the function of this model to simulate blood flow and pressure variations, the question of how to systematically quantify the consequences of these uncertainties in blood pressure arises. Considering the contribution of the article which is limited to the Windkessel model for the cardiovascular system, one may categorize this research as a contribution to the aleatoric uncertainty quantification of the Windkessel model.

Before embarking on a systematic aleatory uncertainty quantification (UQ) of the WK model, one may divide this model's variability into two classes: (i) UQ of the state variables and (ii) UQ of the WK parameters. The former finds the uncertainties of the blood pressure for a known set of statistical properties of the WK parameters and blood flow waveform. The latter discusses how pressure and flow measurement errors will spread to the WK parameters while estimating them through the so-called inverse problems. Given that the WK model mimics the blood flow dynamics, any of the two types of model variability can help assess the reliability of associated decisions drawn based on this model. For example, greater uncertainty in blood pressure measurement corresponds to decreased reliability in clinical decisions derived from them, and vice versa. This research focuses on the former type of variability, meaning we aim to quantify the uncertainty of the pressure waveform (specifically, the systolic, diastolic, and pulse pressures) subject to the variability of the arterial compliance, resistance, characteristic impedance, and flow waveform. Although

subjective (non-quantitative) trends resulting from each parameter's variation are well understood,[1] the development of simple quantitative techniques for predicting pressure uncertainties is yet to be established.

The literature offers several attempts to enhance the knowledge of the UQ of the blood pressure and flow waveform. For example, Chen et al.[15] quantified uncertainties from various sources in the human cardiovascular system based on stochastic simulation of a one-dimensional (1D) arterial network. Quicken et al.[16] presented an adaptive generalized polynomial chaos expansion and applied it to a three-dimensional (3D) abdominal aortic aneurysm wall mechanics model and a 3D model of flow through an arteriovenous fistula. While both studies provide valuable contributions to the quantification of hemodynamic uncertainty, their focus has been on the development of UQ methods tailored for sophisticated models for arterial networks and 3D simulations, hereby considering nonlinear, non-additive and non-monotone relationships between model inputs and outputs. Lee et al.[17] used a Bayesian approach to determine ratios of systolic and diastolic oscillometric amplitude to the mean arterial pressure. Turner et al.[18] used a Monte Carlo simulation to estimate the effects of the sphygmomanometer error and the day-to-day variability of the pressure measurements on the detection of hypertension. Other researchers, for example, Xiu and Sherwin,[19] did not directly investigate the uncertainty of the blood pressure waveform but concentrated on the pulse wave velocity, which is another important indicator of cardiovascular health. Although all these methods offer promising methodologies to predict uncertainties, they can be computationally intensive and time-consuming, especially when dealing with high-dimensional problems and large data sets. Specifically, the Bayesian methods involve repeated simulations of the model for different parameter values, which is computationally expensive.

Despite its simplicity, the WK model is convenient for describing the arterial system. For example, it has been used to evaluate arterial compliance,[1] an important biophysical marker of the arterial wall related to vascular aging,[2] to study the cardiac pump function,[20] and to simulate the load in an artificial heart and valve studies.[21,22] Windkessel models can be divided into mono-compartment and multi-compartment.[23] The main advantages of multi-compartment models are that they are computationally efficient and require few parameters. Such models have been used to estimate different cardiovascular parameters. For example, they were used to assess the elasticity of blood vessels from photoplethysmography measurements[24] or to evaluate oxygen consumption.[25] Different works have used the WK model as boundary conditions in terminal vessels of 1D and 3D models.[2,26–32] To estimate the Windkessel parameters, distinct methods like vector fitting[27] and optimization[28,30] have been used. Such methods allow the incorporation of patient-specific data. In addition, various uncertainty quantification methods, like generalized polynomial chaos,[26] Monte Carlo[29] or first order second moment,[31] have been employed to propagate uncertainties due to the Windkessel boundary conditions and to analyze the effect of uncertain wall elasticity on flow and arterial area variations.[28]

The numerous recent works on the WK model, for example,[23,29,33–37] demonstrate the increasing interest and importance of uncertainty quantification in blood pressure waveform analysis for improved cardiovascular risk assessment and personalized healthcare. Recent advancements in medical imaging, computational power, and the availability of physiological signals have allowed the incorporation of patient-specific data into simulations, which involves uncertainties and potential errors that require evaluation to ensure the reliability of cardiovascular models in clinical practice.[23,35,38,39] Patient-specific models have gained interest in the medical industry, and assessment of their reliability and credibility requires verification, validation, and uncertainty quantification (VVUQ).[23,39–41] This paper aims to develop an efficient and easy-to-implement UQ method based on a local gradient-based formulation to quantify the uncertainty of the pressure waveform resulting from aleatory uncertainties of the WK parameters and flow waveform. The proposed UQ framework was verified against Monte Carlo simulations. To establish the applicability of the formulation, we analyzed an extensive data set constructed based on a comprehensive literature review[42] and compared uncertainties—of the SBP and DBP in different age groups—computed with the proposed formulation, with those observed in vivo and in silico data. Furthermore, we analyzed the uncertainty variation of SBP and DBP due to variations in the uncertainty of WK parameters and extended the UQ formulation to the pulse pressure.

2 | MATERIALS AND METHODS

2.1 | Windkessel model

The two-element WK model adopts resistance, R, relating outflow to pressure difference at either side of the component and compliance, C, denoting the ratio of a volume variation and the resulting pressure change. An

improved version of the two-parameter WK model incorporates another resistive element, Z, to account for the characteristic impedance of the vessels, that is, the impedance obtained from the input impedance spectrum at high frequencies when no reflections exist.[1] Assuming the flow rate $Q(t)$ through the ascending aorta as uncertain input and the aforementioned WK parameters as random quantities, the aortic blood pressure $P(t)$ is evaluated from Reference 43.

$$P + RC\frac{dP}{dt} = (R+Z)Q + ZRC\frac{dQ}{dt} + P_{\text{out}}, \tag{1}$$

where P_{out} is an asymptotic pressure representing the venous pressure.

Equation (1) can be solved using the integrating factor method, leading to.

$$P(t) = ZQ(t) + \frac{1}{C}e^{-\frac{t}{RC}}\int_0^{t'} e^{\frac{t'}{RC}}Q(t')dt' + (P_D - P_{\text{out}})e^{-\frac{t}{RC}} + P_{\text{out}}, \tag{2}$$

with P_D is the diastolic blood pressure. This WK model can reduce the entire arterial network or part of it into a lumped parameter model. In this work, the flow rate at the aorta was used to quantify the corresponding pressure, implying that the employed WK parameters are for the entire arterial network.

2.2 | Uncertainty propagation to the aortic pressure

The aim of this study was to estimate the uncertainty of the pressure waveform subject to uncertain input WK parameters and flow waveform. Following the work done by Charlton et al.,[42] the flow rate morphology was modeled to give reasonable pulse wave simulations. In Charton's work the morphology of the flow wave is influenced by heart rate (HR), stroke volume (SV), left ventricular ejection time, peak flow time, and reverse flow volume. We used the scrip AorticFlowWave, developed by Charlton et al.,[42] which produces a flow waveform given a set of cardiac parameters. To illustrate how uncertainties of flow waveform propagate to the pressure, we introduced uncertainties in the flow waveform through variations of the SV and HR. The state variable $P(t)$ is the solution of the ordinary differential equation (ODE) shown in Equation (1), which due to uncertain parameters and flow waveform, is stochastic in nature.

Uncertainty analysis methods may be classified as probabilistic and non-probabilistic approaches.[44] Belonging to the former category, Monte Carlo is a simulation-based method used in this research to verify the proposed stochastic formulations. The most efficient non-probabilistic techniques are local expansion-based methods, such as the Taylor series (employed herein) and perturbation method.[45–47] These methods are only robust for cases of relatively small input variability and (relatively) linear models, which is the case of WK models. The next section introduces our proposed expansion-based formulation.

2.3 | Estimation of the pressure variance

Let the random vector $\boldsymbol{X} = (R, C, Z, SV, HR)^T$ define the WK (R, C, Z) and cardiac (SV, HR) parameters with covariance matrix

$$\text{cov}[\boldsymbol{X},\boldsymbol{X}] = \mathbb{E}\left[(\boldsymbol{X}-\bar{\boldsymbol{X}})(\boldsymbol{X}-\bar{\boldsymbol{X}})^T\right] = \begin{bmatrix} \sigma_R^2 & \text{cov}(R,C) & \text{cov}(R,Z) & \text{cov}(R,SV) & \text{cov}(R,HR) \\ \text{cov}(C,R) & \sigma_C^2 & \text{cov}(C,Z) & \text{cov}(C,SV) & \text{cov}(C,HR) \\ \text{cov}(Z,R) & \text{cov}(Z,C) & \sigma_Z^2 & \text{cov}(Z,SV) & \text{cov}(Z,HR) \\ \text{cov}(SV,R) & \text{cov}(SV,C) & \text{cov}(SV,Z) & \sigma_{SV}^2 & \text{cov}(SV,HR) \\ \text{cov}(HR,R) & \text{cov}(HR,C) & \text{cov}(HR,Z) & \text{cov}(HR,SV) & \sigma_{HR}^2 \end{bmatrix} \tag{3}$$

where $\bar{\boldsymbol{X}} = \mathbb{E}(\boldsymbol{X})$, $\mathrm{cov}\left[X_i, X_j\right], i,j = 1,2,3,4,5$ stands for the covariance between variables X_i and X_j and $\sigma_X^2 = \mathrm{var}[X_i]$. Our methodology considers that the WK and cardiac parameters are uncorrelated. Therefore, off-diagonal terms are equal to zero in the covariance matrix. Taylor series analysis allows for the following expansion of the pressure waveform,

$$P(\boldsymbol{X}) = P(\bar{\boldsymbol{X}}) + \sum_{i=1}^{5} \frac{\partial P}{\partial X_i}\bigg|_{\bar{\boldsymbol{X}}} (X_i - \bar{X}_i) + \sum_{i=1}^{5} \frac{\partial^2 P}{\partial X^2{}_i}\bigg|_{\bar{\boldsymbol{X}}} \frac{(X_i - \bar{X}_i)^2}{2!} + \ldots. \tag{4}$$

By neglecting nonlinear terms, the variance of the pressure at each time step can be calculated as

$$\mathbb{E}\left[\left(P(\boldsymbol{X}) - P(\bar{\boldsymbol{X}})\right)^2\right] = \sum_{j=1}^{5} \sum_{i=1}^{5} \frac{\partial P}{\partial X_i}\bigg|_{\bar{\boldsymbol{X}}} \frac{\partial P}{\partial X_j}\bigg|_{\bar{\boldsymbol{X}}} \mathbb{E}\left[\left(X_i - \bar{X}_i\right)\left(X_j - \bar{X}_j\right)\right], \tag{5}$$

or

$$\sigma_P^2 = \left[\frac{\partial P(\bar{\boldsymbol{X}})}{\partial R} \frac{\partial P(\bar{\boldsymbol{X}})}{\partial C} \frac{\partial P(\bar{\boldsymbol{X}})}{\partial Z} \frac{\partial P(\bar{\boldsymbol{X}})}{\partial SV} \frac{\partial P(\bar{\boldsymbol{X}})}{\partial HR}\right] \mathrm{cov}[\boldsymbol{X},\boldsymbol{X}] \left[\frac{\partial P(\bar{\boldsymbol{X}})}{\partial R} \frac{\partial P(\bar{\boldsymbol{X}})}{\partial C} \frac{\partial P(\bar{\boldsymbol{X}})}{\partial Z} \frac{\partial P(\bar{\boldsymbol{X}})}{\partial SV} \frac{\partial P(\bar{\boldsymbol{X}})}{\partial HR}\right]^T. \tag{6}$$

Note that the gradient vector pre-multiplying and post-multiplying the covariance matrix is deterministic, since it is evaluated based on the pressure waveform which itself is quantified based on the WK and cardiac parameters. In Equation (6), we assume a priori knowledge of the covariance matrix for the WK and cardiac parameters. This knowledge may be achieved through different methods, depending on the context and available data. For example, one way to estimate the covariance matrix is to use historical data or experimental measurements and use statistical analysis techniques to estimate the covariance matrix from this data.[48] Another approach is to use expert knowledge or prior information about the system and its parameters to estimate the covariance matrix. In this case, the covariance matrix may be based on physical principles or previous studies of similar systems.[49]

The numerical evaluation of the pressure gradients with respect to the WK parameters and flow waveform determinants, as shown in Equation (6), is described in the following section.

2.4 | Evaluation of sensitivities

This section aims to estimate the gradients in Equation (6) using an efficient numerical approach. The numerical methods approximate the ODE solution at discrete points in time. Common numerical methods for this purpose include the Euler and Runge–Kutta methods used to obtain accurate and efficient solutions to a wide range of ODE problems.[50] In this study, the Euler method which constitutes the simplest scheme to solve the ODE in Equation (1) is implemented.[50] Considering a known time history of flow rate at the aorta, the computational solution to pressure reads

$$P(t + \Delta t) = \frac{\alpha \Delta t + RCP(t)}{\Delta t + RC},$$

$$\alpha(\mathrm{t}) = (R + Z)Q(t + \Delta t) + ZRC\frac{Q(t + \Delta t) - Q(t)}{\Delta t} + P_{\mathrm{out}}. \tag{7}$$

The provided expression for the pressure can now be differentiated with respect to each of the WK parameters to arrive at the desired sensitivity. Consider $\partial Q(\partial R)^{-1} = 0, \partial Q(\partial C)^{-1} = 0, \mathrm{and} \partial Q(\partial Z)^{-1} = 0$, since the flow waveform is just a function of SV and HR. The expressions for the pressure gradient with respect to R then reduce to

$$\frac{\partial P}{\partial R}(t + \Delta t) = \frac{\left(\frac{\partial \alpha}{\partial R}\Delta t + CP(t) + RC\frac{\partial P}{\partial R}(t)\right)(\Delta t + RC) - C(\alpha \Delta t + RCP(t))}{(\Delta t + RC)^2},$$

$$\text{with}\frac{\partial\alpha}{\partial R}=Q(t+\Delta t)+ZC\frac{Q(t+\Delta t)-Q(t)}{\Delta t}. \tag{8}$$

where $\partial P(\partial R)^{-1}(t)$ is the estimated gradient at the previous time step. Therefore, all variables are known quantities. Likewise, the pressure derivative with respect to C is

$$\frac{\partial P}{\partial C}(t+\Delta t)=\frac{\left(\frac{\partial\alpha}{\partial C}\Delta t+RP(t)+RC\frac{\partial P}{\partial C}(t)\right)(\Delta t+RC)-R(\alpha\Delta t+RCP(t))}{(\Delta t+RC)^2},$$

$$\text{with}\frac{\partial\alpha}{\partial C}=ZR\frac{Q(t+\Delta t)-Q(t)}{\Delta t}. \tag{9}$$

Finally, the sensitivity of pressure with respect to Z yields:

$$\frac{\partial P}{\partial Z}(t+\Delta t)=\frac{1}{\Delta t+RC}\left(\frac{\partial\alpha}{\partial Z}\Delta t+RC\frac{\partial P}{\partial Z}(t)\right), \tag{10}$$

with

$$\frac{\partial\alpha}{\partial Z}=Q(t+\Delta t)+RC\frac{Q(t+\Delta t)-Q(t)}{\Delta t}. \tag{11}$$

The sensitivity of the pressure with respect the cardiac variables $\left(\frac{\partial P}{\partial SV},\frac{\partial P}{\partial HR}\right)$ is given by.

$$\frac{\partial P}{\partial SV}=\frac{\partial P}{\partial Q}\frac{\partial Q}{\partial SV}\text{and}\frac{\partial P}{\partial HR}=\frac{\partial P}{\partial Q}\frac{\partial Q}{\partial HR}. \tag{12}$$

Using Equation (7) we have that.

$$\frac{\partial P(t+\Delta t)}{\partial Q}=\frac{\frac{\partial\alpha}{\partial Q}\Delta t+RC\frac{\partial P(t)}{\partial Q}}{\Delta t+RC},\text{with}\frac{\partial\alpha}{\partial Q}=(R+Z). \tag{13}$$

The AorticFlowWave script[42] provided data to compute the derivatives of the flow with respect to the cardiac variables $\left(\frac{\partial Q}{\partial SV},\frac{\partial Q}{\partial HR}\right)$ that are required to calculate Equation (12). Substitution of Equations (8), (9), (10), and (12) into Equation (6) (along with the covariance matrix) allows one to compute the pressure standard deviation for the expansion-based method.

2.5 | Stochastic properties of the Windkessel and cardiac parameters

To show how the uncertainty of the WK and cardiac parameters propagates to the pressure waveform, especially to the systolic, diastolic, and pulse pressures, a sensible set of values for the statistical properties of the WK and cardiac parameters are required. To this end, we used an existing database containing in silico pressure and flow waves at the aortic root in a group of 4374 virtual subjects.[42] Pulse waves were simulated using a 116-artery 1D model of blood flow in the larger systemic arteries of the thorax, limbs, and head. Charlton et al.[42] considered a wide range of typical cardiovascular variables of healthy adults aged 25 to 75. Such cardiovascular properties were identified through a comprehensive literature review, and simulated waves were verified by comparison against in vivo data. Six cardiovascular variables (HR, SV, left ventricular ejection time, arterial diameter, pulse wave velocity, and mean arterial pressure) that strongly influenced the pulse waves were varied independently by ± one standard deviation at each decade, that is, for each decade $3^6=729$ virtual subjects were considered giving a total of $6\times729=4{,}374$ virtual subjects. Following Charlton et al.,[42] virtual subjects with abnormal pulse pressure or its amplification were discriminated against.

We assessed the parameters of the WK model for each virtual subject as follows: the database provides the pulse wave velocity (PWV), aortic area (A_o), blood density (ρ), outflow pressure (P_{out}), and time decay in diastole ($\tau = RC$). Using this information, we computed the characteristic impedance as[19]

$$Z = \frac{\rho PWV}{A_o}. \tag{14}$$

For one cardiac cycle with a period T, the total resistance (R_T) was calculated based on the average pressure $\left(\overline{P} = \frac{1}{T}\int_0^T P(t)dt\right)$, the mean flow rate $\left(\overline{Q} = \frac{1}{T}\int_0^T Q(t)dt\right)$ and the outflow pressure P_{out}, that is,

$$R_T = \frac{\overline{P} - P_{\text{out}}}{\overline{Q}}. \tag{15}$$

The peripheral resistance and compliance were calculated as.

$$R = R_T - Z \text{and} C = \frac{\tau}{R}. \tag{16}$$

Once the foregoing calculations were implemented for each individual virtual subject, the statistical properties of the WK parameters were estimated. Table 1 shows the mean values and standard deviations (STD) of the WK parameters for each age decade.

Influence of the variability of the flow waveform was investigated by using the AorticFlowWave script[42] to reproduce representative flow waveforms from data of the SV, HR, left ventricle ejection time (LVET), peak flow time, reverse flow volume, and flow wave morphology.[42] However, to simplify the methodology and results interpretability, we selected two determinants of the flow waveform: the SV and HR.

2.6 | Uncertainty analysis of the pulse pressure

Pulse pressure (PP), defined as the difference between systolic and diastolic pressure, may indicate cardiovascular disease; for instance, elevated pulse pressure is recognized as a risk factor for coronary disease.[51] Therefore, measuring pulse pressure is important to assess a patient's cardiovascular health and to make informed decisions about their treatment plan.

Due to the clinical relevance of PP, propagation of the uncertainty of the WK and cardiac parameters to PP is an important task. The expansion-based method allows us to assess an approximated PP variance. The variance of the PP can be calculated as

$$\sigma_{PP}^2 = \mathbb{E}\left[\left(P_S(\boldsymbol{X}) - P_D(\boldsymbol{X})\right)^2\right] - \left(P_S(\bar{\boldsymbol{X}}) - P_D(\bar{\boldsymbol{X}})\right)^2$$

TABLE 1 Windkessel parameters of the database; values are mean ± standard deviation; n is the number of virtual subjects in an age group.

Age decade	R (mmHg·s/mL)	C (mL/mmHg)	Z (mmHg·s/mL)
25 ($n = 712$)	0.6632 ± 0.1622	1.7389 ± 0.3472	0.0409 ± 0.0073
35 ($n = 684$)	0.6909 ± 0.1772	1.5495 ± 0.3900	0.0419 ± 0.0081
45 ($n = 654$)	0.7501 ± 0.1902	1.3086 ± 0.3047	0.0442 ± 0.0085
55 ($n = 641$)	0.7844 ± 0.2055	1.1177 ± 0.2769	0.0465 ± 0.0092
65 ($n = 588$)	0.8152 ± 0.2206	0.9503 ± 0.2502	0.0485 ± 0.0099
75 ($n = 558$)	0.8611 ± 0.2264	0.7997 ± 0.2539	0.0512 ± 0.0108

$$= \sigma_S^2 + \sigma_D^2 - 2(\mathbb{E}[P_S(\boldsymbol{X})P_D(\boldsymbol{X})] - P_S(\bar{\boldsymbol{X}})P_D(\bar{\boldsymbol{X}})), \tag{17}$$

where P_S is the systolic pressure and σ_S and σ_D are the standard deviations of the systolic and diastolic pressures, respectively. Note that $\mathbb{E}[P_S(\boldsymbol{X})] = P_S(\bar{\boldsymbol{X}})$, $\mathbb{E}[P_D(\boldsymbol{X})] = P_D(\bar{\boldsymbol{X}})$, and $\mathbb{E}[\boldsymbol{X}] = \bar{\boldsymbol{X}}$.

The last term in Equation (17) represents the covariance between the systolic and diastolic pressures, that is,

$$\mathbb{E}[P_S(\boldsymbol{X})P_D(\boldsymbol{X})] - P_S(\bar{\boldsymbol{X}})P_D(\bar{\boldsymbol{X}}) = \mathrm{cov}[P_S, P_D] = \mathbb{E}[(P_S(\boldsymbol{X}) - P_S(\bar{\boldsymbol{X}}))(P_D(\boldsymbol{X}) - P_D(\bar{\boldsymbol{X}}))] \tag{18}$$

This term can be quantified using pressure gradients. The Taylor series for the systolic and diastolic pressures are given by

$$P_S(\boldsymbol{X}) = P_S(\bar{\boldsymbol{X}}) + \sum_{i=1}^{5} \frac{\partial P_S}{\partial X_i}\bigg|_{\bar{\boldsymbol{X}}} (X_i - \bar{X}_i) + \sum_{i=1}^{5} \frac{\partial^2 P_S}{\partial X_i^2}\bigg|_{\bar{\boldsymbol{X}}} \frac{(X_i - \bar{X}_i)^2}{2!} + \ldots. \tag{19}$$

$$P_D(\boldsymbol{X}) = P_D(\bar{\boldsymbol{X}}) + \sum_{i=1}^{5} \frac{\partial P_D}{\partial X_i}\bigg|_{\bar{\boldsymbol{X}}} (X_i - \bar{X}_i) + \sum_{i=1}^{5} \frac{\partial^2 P_D}{\partial X_i^2}\bigg|_{\bar{\boldsymbol{X}}} \frac{(X_i - \bar{X}_i)^2}{2!} + \ldots. \tag{20}$$

By neglecting nonlinear terms and moving $P_S(\bar{\boldsymbol{X}})$, and $P_D(\bar{\boldsymbol{X}})$ to the left-hand side of Equations (19) and (20), respectively, we can approximate the product of the systolic and diastolic pressure deviation from their mean as

$$(P_S(\boldsymbol{X}) - P_S(\bar{\boldsymbol{X}}))(P_D(\boldsymbol{X}) - P_D(\bar{\boldsymbol{X}})) = \sum_{j=1}^{5} \sum_{i=1}^{5} \frac{\partial P_S}{\partial X_i}\bigg|_{\bar{\boldsymbol{X}}} \frac{\partial P_D}{\partial X_j}\bigg|_{\bar{\boldsymbol{X}}} (X_i - \bar{X}_i)(X_j - \bar{X}_j). \tag{21}$$

The expectation of the resultant expression in Equation (21) yields.

$$\begin{aligned}\mathrm{cov}[P_S, P_D] &= \mathbb{E}\left[\left(P_S(\boldsymbol{X}) - P_S\left(\bar{\boldsymbol{X}}\right)\right)\left(P_D(\boldsymbol{X}) - P_D\left(\bar{\boldsymbol{X}}\right)\right)\right] = \sum_{j=1}^{5} \sum_{i=1}^{5} \frac{\partial P_S}{\partial X_i}\bigg|_{\bar{\boldsymbol{X}}} \frac{\partial P_D}{\partial X_j}\bigg|_{\bar{\boldsymbol{X}}} \mathbb{E}\left[\left(X_i - \bar{X}_i\right)\left(X_j - \bar{X}_j\right)\right] \\ &= \left[\frac{\partial P_S\left(\bar{\boldsymbol{X}}\right)}{\partial R} \frac{\partial P_S\left(\bar{\boldsymbol{X}}\right)}{\partial C} \frac{\partial P_S\left(\bar{\boldsymbol{X}}\right)}{\partial Z} \frac{\partial P_S\left(\bar{\boldsymbol{X}}\right)}{\partial LV} \frac{\partial P_S\left(\bar{\boldsymbol{X}}\right)}{\partial HR}\right] \mathrm{cov}[\boldsymbol{X}, \boldsymbol{X}] \left[\frac{\partial P_D\left(\bar{\boldsymbol{X}}\right)}{\partial R} \frac{\partial P_D\left(\bar{\boldsymbol{X}}\right)}{\partial C} \frac{\partial P_D\left(\bar{\boldsymbol{X}}\right)}{\partial Z} \frac{\partial P_S\left(\bar{\boldsymbol{X}}\right)}{\partial LV} \frac{\partial P_S\left(\bar{\boldsymbol{X}}\right)}{\partial HR}\right]^T.\end{aligned} \tag{22}$$

Substitution of Equation (22) into Equation (17) leads.

$$\begin{aligned}\sigma_{PP}^2 = \sigma_S^2 + \sigma_D^2 - 2 &\left[\frac{\partial P_S\left(\bar{\boldsymbol{X}}\right)}{\partial R} \frac{\partial P_S\left(\bar{\boldsymbol{X}}\right)}{\partial C} \frac{\partial P_S\left(\bar{\boldsymbol{X}}\right)}{\partial Z} \frac{\partial P_S\left(\bar{\boldsymbol{X}}\right)}{\partial LV} \frac{\partial P_S\left(\bar{\boldsymbol{X}}\right)}{\partial HR}\right] \\ &\mathrm{cov}[\boldsymbol{X}, \boldsymbol{X}] \left[\frac{\partial P_D\left(\bar{\boldsymbol{X}}\right)}{\partial R} \frac{\partial P_D\left(\bar{\boldsymbol{X}}\right)}{\partial C} \frac{\partial P_D\left(\bar{\boldsymbol{X}}\right)}{\partial Z} \frac{\partial P_S\left(\bar{\boldsymbol{X}}\right)}{\partial LV} \frac{\partial P_S\left(\bar{\boldsymbol{X}}\right)}{\partial HR}\right]^T.\end{aligned} \tag{23}$$

Equation (23) offers an efficient formula to quantify the variance of the pulse pressure based on the variance of the systolic pressure σ_S^2, the variance of the diastolic pressure σ_D^2, the covariance matrix of the WK and cardiac parameters, that is, $\mathrm{cov}[\boldsymbol{X}, \boldsymbol{X}]$, and the gradient of the systolic and diastolic pressures. The latter can be quantified based on the formulations developed in Section 2.4; note that the gradient values corresponding to the systolic and diastolic pressures must be selected from the gradient vectors.

2.7 | Verification of the proposed method

The proposed numerical formulation was verified against the exhaustive Monte Carlo simulations. Four different values of the standard deviation of the WK and cardiac parameters were tested: 0, 2.5, 5, and 10% of the mean values, making a total of 16 simulations. The mean values of the cardiac parameters are SV = 66.8 mL and HR = 75 beats/min. The first row of Table 1 shows the mean values of the WK parameters. In the Monte Carlo method, Equation (1) was solved 15,000 times (for each simulation) using WK and cardiac parameters taken randomly from normal distributions. No correlation between the variables was considered. For each simulation, collecting 15,000 solutions enables computing the standard deviation and mean value at each time point using the 15,000 pressure samples. For that number of samples, convergence of the mean pressure and its standard deviation was achieved. We used Equation (6) for the expansion-based method with the pressure derivatives given by Equations (8), (9), (10), and (12). The results of both methods were compared using the root mean square error (RMS) defined as

$$\varepsilon^{\pm} = \sqrt{\frac{1}{n}\sum_{i=1}^{n}\left(\frac{[P_i \pm \sigma_i]_{EB} - [P_i \pm \sigma_i]_{MC}}{[P_i \pm \sigma_i]_{MC}}\right)^2}, \tag{24}$$

where n is the number of temporal points in one cardiac cycle, $[P_i \pm \sigma_i]_{EB}$ is the pressure plus and minus the standard deviation (σ) obtained with the expansion-based method at the time point i. At the same time, $[P_i \pm \sigma_i]_{MC}$ is the pressure plus and minus the STD from Monte Carlo simulations.

2.8 | Uncertainty assessment of the aortic systolic and diastolic pressure

We illustrated the applicability of our uncertainty propagation method in two scenarios. In the first one, the parameters of the WK model are known (as for each decade in the database) and are used to assess variations in SBP and DBP. To do so, we propagated the uncertainties due to the WK parameters for each virtual subject with Equation (6) and extracted the SBP ± STD and DBP ± STD. Moreover, we assessed the PP and its STD using Equation (23). To compare our results with those of the in silico database,[42] for each virtual subject, we collected the aortic systolic, diastolic, and pulse pressures. Then, by decades, we calculate their means and standard deviations. Furthermore, we compared the results with in vivo data for each age decade from the literature.[52] In vivo data corresponds to the Anglo-Cardiff Collaborative Trial (ACCT), which consists of 10,096 individuals selected randomly from local General Practice lists and open-access Cardiovascular Risk Assessment Clinics across East Anglia and Wales. Only data for healthy subjects were selected, giving a total of 4001 individuals for the analysis.[52]

In the second scenario, the uncertainty variation of SBP and DBP due to variations in the uncertainty of WK parameters was analyzed. To do so, we used as reference values the STD of the WK parameters of the first row of Table 1. In this scenario, one can determine the variables making considerable changes in SBP and DBP.

3 | RESULTS

Figure 1 shows the standard deviations obtained from Monte Carlo simulations (shaded areas) and, those of the proposed method (i.e., the expansion-based approach; in dotted blue lines). When the flow waveform has no uncertainties (first column), both methodologies produced similar uncertainties at all time points of the pressure waveform and values of the WK standard deviations, with RMS errors smaller than 0.5%. However, when only propagating the uncertainty due to the flow waveform (second row of Figure 1), the expansion-based method partially propagated the uncertainty of the flow waveform, that is, in systole, it overestimated and underestimated the upper and lower STD boundaries, respectively, and in diastole was not able to reproduce uncertainties, resulting in RMS errors of ∼10% with increasing STD of the cardiac parameters. The expansion-base method results deviate from those of Monte Carlo simulations as the STD of the cardiac parameters increases. To easily compare the signals, we used the same time interval in all subplots. This makes the changes in heart rate less obvious, but they can still be seen at the end of the signals. For instance, see the last column and third row, where the standard deviation diminishes due to the variation in the signal duration. Our results indicate that the proposed method produces accurate pressure STDs when uncertainties steaming

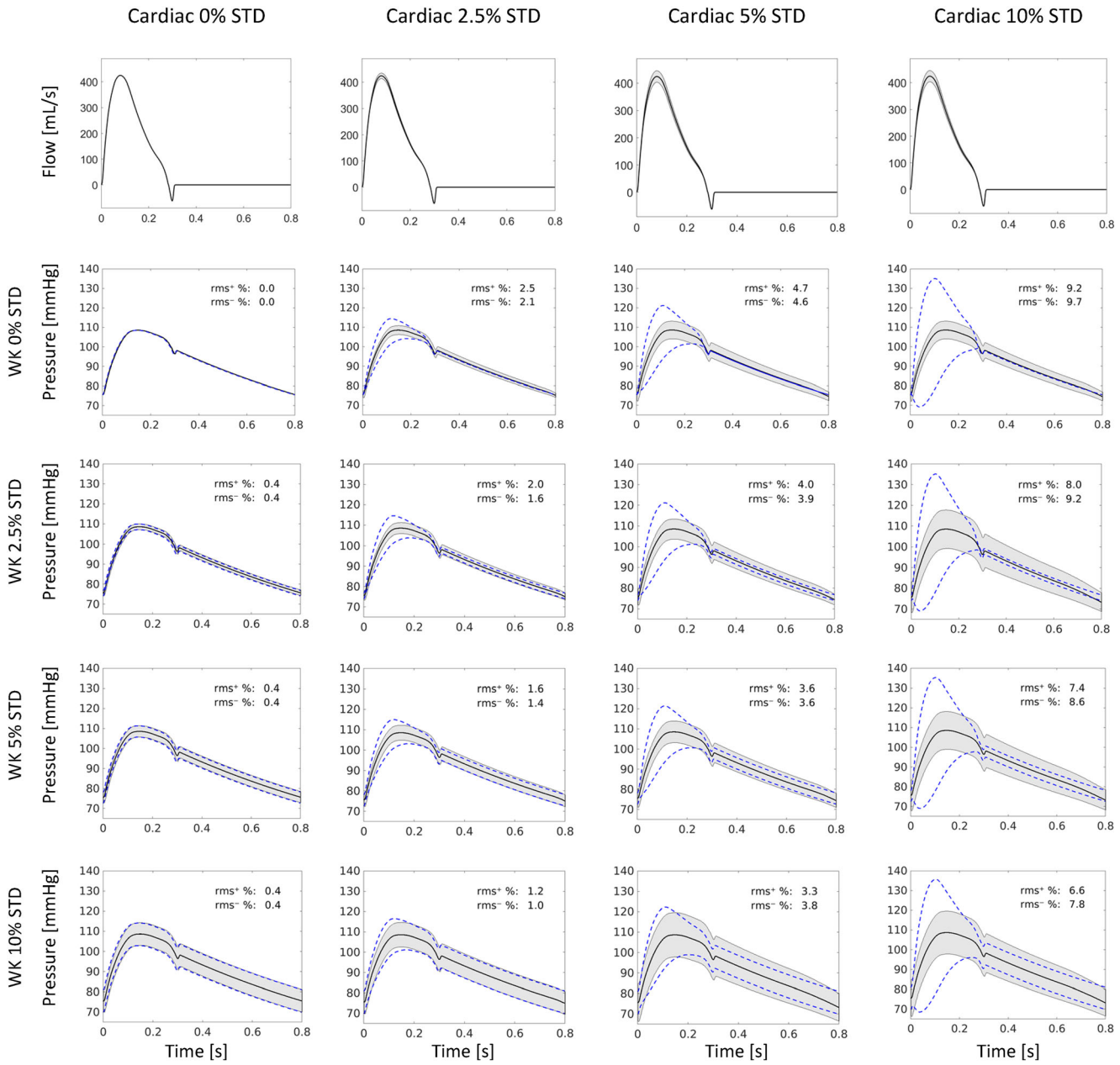

FIGURE 1 Verification of the proposed uncertainty quantification method. The first row shows the mean and standard deviation (STD) of the blood flow waveform due to variations of the stroke volume and heart rate STD from 0% to 10% of the mean value, which correspond to those of the 25-year-old baseline subject, namely, 66.8 mL and 75 beats/min,[42] respectively. The Windkessel (WK) parameters' standard deviation varies from 0 to 10% of the mean value from the second to the fifth row; the mean values correspond to WK parameters shown in the first row of Table 1. The resulting mean pressure and STD from Monte Carlo simulations are shown in black lines and shadows, respectively. The blue line is the STD obtained with the proposed expansion-based method (Equation 6). Root means square errors computed with Equation (24) are shown in each plot.

from the blood flow waveform are considerably smaller than those of the WK parameters; see, for instance, the last two rows of the second column of Figure 1, where RMS errors are smaller than 2%.

3.1 | Uncertainty of the aortic systolic and diastolic pressure

In this section, the applicability of our uncertainty propagation method is illustrated in two scenarios. We only propagated uncertainties steaming from the Windkessel parameters because the expansion-base method gives the most accurate results in this situation.

3.2 | Uncertainty quantification of the systolic and diastolic pressures

For the first scenario, the uncertainty in the pressure waveform at each decade is investigated. Mean values and STD of the WK parameters for each age decade, shown in Table 1, were used to calculate the pressure waveform and its uncertainties through Equations (2) and (6), respectively. As depicted in Figure 2, the aortic pressure waveform and their uncertainties for decades 25 and 75 are presented based on the data provided by Charlton et al.[42] The aortic pressure waveforms and their uncertainties for the rest of the decades (from 35 to 65) are shown in Appendix A. The Windkessel model reproduces similar pressure waveforms to those of the virtual subjects with root-mean-square errors smaller than 5% for all decades.

Figure 3C shows the systolic, diastolic, and pulse pressures, along with their STD, for the expansion-based method. The STD for the SBP and DBP obtained with the expansion-based method follows the trends seen in the database (Figure 3A) and in vivo data (Figure 3B). For example, as age increases, the STD of diastolic and systolic blood pressure also increases in both the database and the expansion-based method (first and second row of Figure 3D). Nonetheless, the expansion-based method leads to higher SBP and DBP standard deviations. Additionally, the pulse pressure increases with age in all cases (third row of Figure 3D).

3.3 | Variations in the standard deviations of the systolic and diastolic pressures

Figure 4 shows that the expansion-based method and Monte Carlo simulations predict similar systolic (Figure 4A) and diastolic (Figure 4B) pressure standard deviations when varying the STD of the Windkessel parameters; however, when the variation of the STD of the compliance is greater than 1.25 times the reference value ($[stdC]_0$), there is a significant difference in the STD of the SBP (see the results in red of Figure 4A), reaching a maximum error of 15%. The maximum error was computed as, $\max\left|\left(STD_i^{EB}-STD_i^{MC}\right)/STD_i^{MC}\right|$, where STD_i^{EB} and STD_i^{MC} are the STD of the expansion-based method and Monte Carlo simulations for the same value (i) of the STD of a Windkessel parameter, respectively. Note that in Figures 4 and 5 the range of the STD of each Windkessel parameter is determined by the reference value. For instance, in Figures 4A,B and 5A the initial and final values of the STD of the peripheral resistance are given by $[stdR]=0.5[stdR]_0=0.0811\text{mmHg}\cdot\text{s/mL}$ and $[stdR]=1.5[stdR]_0=0.2493\text{mmHg}\cdot\text{s/mL}$, respectively. Variation of the standard deviation of the peripheral resistance produces the most significant change in the SBP and DBP uncertainties (see results in black of Figure 4A,B). On the contrary, the variation of the SBP uncertainty due to the uncertainty of the characteristic impedance is insignificant (see the blue dots in Figure 4A), varying only 2.5% from the initial ($stdZ=0.5[stdZ]_0$) to the last value ($stdZ=1.5[stdZ]_0$). In the DBP, variation of the compliance leads to a slight variation of the STD (see the red dots Figure 4B).

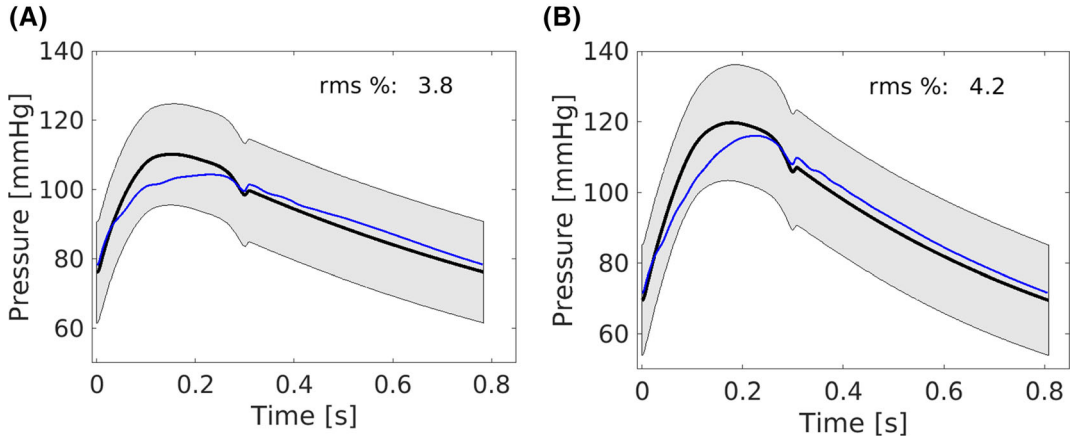

FIGURE 2 Aortic pressure with standard deviations; for (A) 25 and (B) 75 decades. The shaded area shows the standard deviation of pressure obtained with Equation (6). The black line is the pressure for the mean values of the Windkessel parameters. The blue line is the aortic pressure from the in silico database (baseline subject of the decade).[42] The root mean square error with the baseline subject's pressure as a reference is shown in each plot.

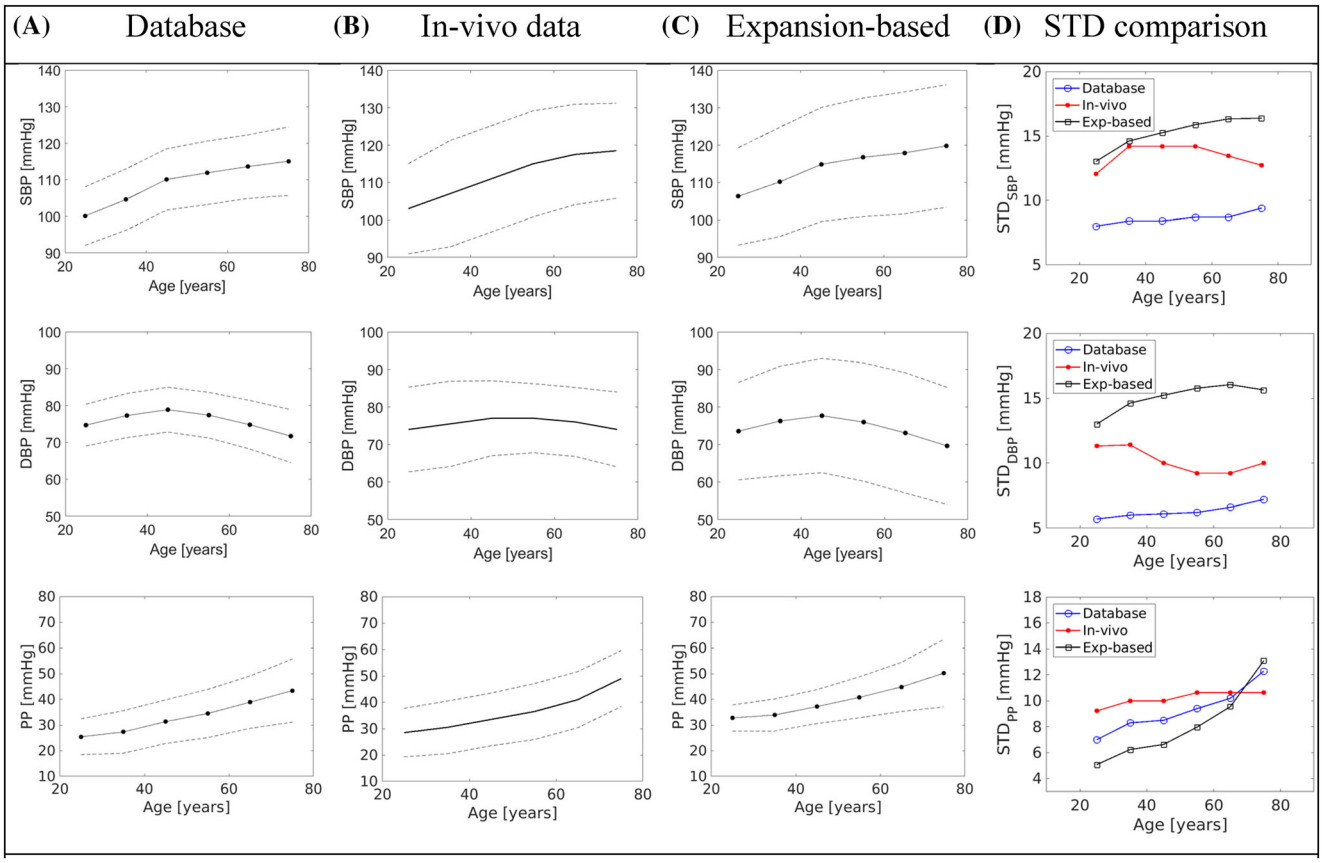

FIGURE 3 Systolic blood pressure (SBP), diastolic blood pressure (SBP) and pulse pressure (PP) variations with age, with standard deviations (STD), for (A) the database, (B) in vivo data, and (C) the current method (obtained with the expansion-based approach). The solid lines indicate mean values, and the dashed lines indicated +/− STD. The in silico and in vivo values were taken from References 42,52, respectively. Column (D) compares the STD for all cases.

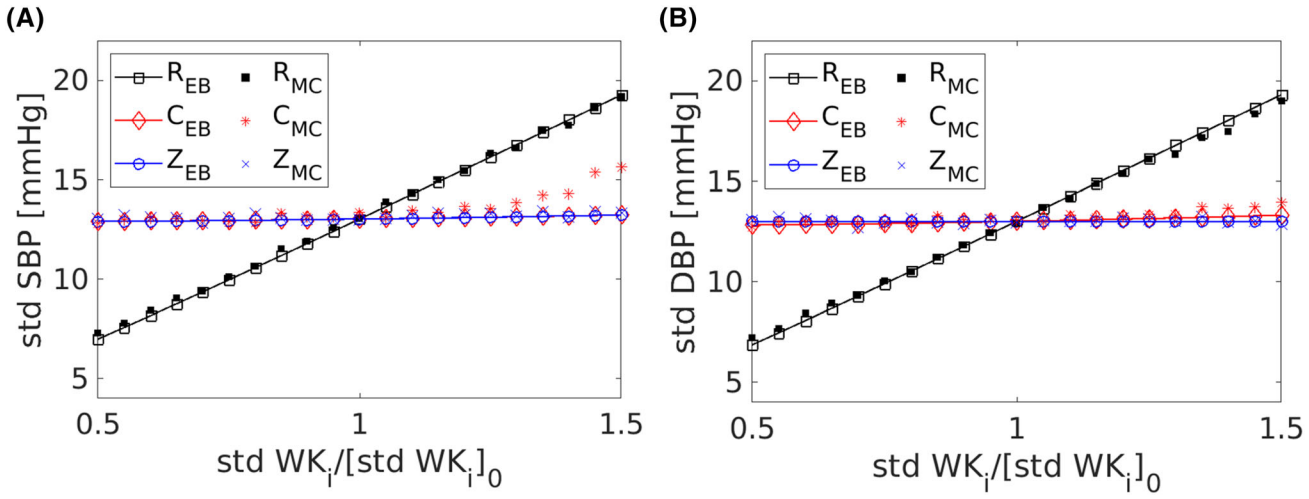

FIGURE 4 Standard deviation of (A) systolic (STD SBP) and (B) diastolic (STD DBP) blood pressures as a function of the standard deviation of a Windkessel parameter ($WK_i = (R,C,Z)$) normalized by a reference value shown in the first row of Table 1 $\left([stdR]_0 = 0.1622\frac{\text{mmHg}\cdot\text{s}}{\text{mL}}, [stdC]_0 = 0.3472\frac{\text{mL}}{\text{mmHg}} \text{and} [stdZ]_0 = 0.0073\text{mmHg}\frac{\text{mmHg}\cdot\text{s}}{\text{mL}}\right)$. Expansion-based method results (EB) are represented by lines with dots and those obtained with Monte Carlo (MC) simulations with dots.

3.4 | Uncertainty analysis of the pulse pressure

Figure 5 shows the uncertainty propagation of the WK parameters to the pulse pressure obtained with Equation (23) (line with dots) and with Monte Carlo simulations (dots). We found that for relatively high variations of the STD of the WK parameters, the expansion-base method describes the tendencies observed in Monte Carlo simulations but with different values (Figure 5A); for instance, the STD of the PP increases as the STD of the compliance does and is almost constant as a function of the STD of the characteristic impedance. When the variations are smaller than 10% of the STD of the WK parameters of the first row of Table 1, both methodologies reproduce similar results (Figure 5B) with maximum errors smaller than 2.5%. Note that the STD range of each Windkessel parameter in Figure 5A,B differs. For example, in Figure 5A, the initial STD value of peripheral resistance is $[stdR] = 0.0811\text{mmHg}\cdot\text{s/mL}$, while in Figure 5B it is $0.00811\text{mmHg}\cdot\text{s/mL}$. We found that the variation of the STD of the compliance produces the most significant change in the PP uncertainty. On the contrary, the peripheral resistance has the least impact on the PP uncertainty.

4 | DISCUSSION

The current research on the Windkessel model is conducted in view of the growing importance of uncertainty quantification in blood pressure waveform, which has the potential to enhance cardiovascular risk assessment and facilitate personalized healthcare. A comprehensive examination of the uncertainty quantification of blood pressure waveforms generated by the Windkessel model enhances the reliability of the model's predictions and contributes to the advancement to patient-specific models and so on the decision-making based on those models. For the quantification of uncertainty in pressure waveform, one potential application lies in the estimation of the pressure waveform using the Windkessel model. Fortunately, the parameters of the Windkessel model correlate with specific physical and patient-specific factors, e.g. compliance correlates with pulse wave velocity. This correlation enables the estimation of these parameters, albeit with a certain degree of uncertainty. Consequently, this introduces a critical question regarding the validity of the estimated pressure waveform, particularly when sensor data are utilized to determine these Windkessel parameters. It is essential to assess the level of confidence in these estimations to ensure that the resulting pressure waveform reflects an accurate representation of the patient's cardiovascular status. This question has been partly answered in the present article.

In this study, we have developed a local gradient-based approach to determine the uncertainty of the pressure waveform that results from the Windkessel parameters and aortic flow waveform. The proposed uncertainty quantification framework is verified through comparison with Monte Carlo simulations. Furthermore, to demonstrate the practicality of our formulation, we have analyzed extensive in silico data sets from recent literature, in addition to comparisons against in vivo data.

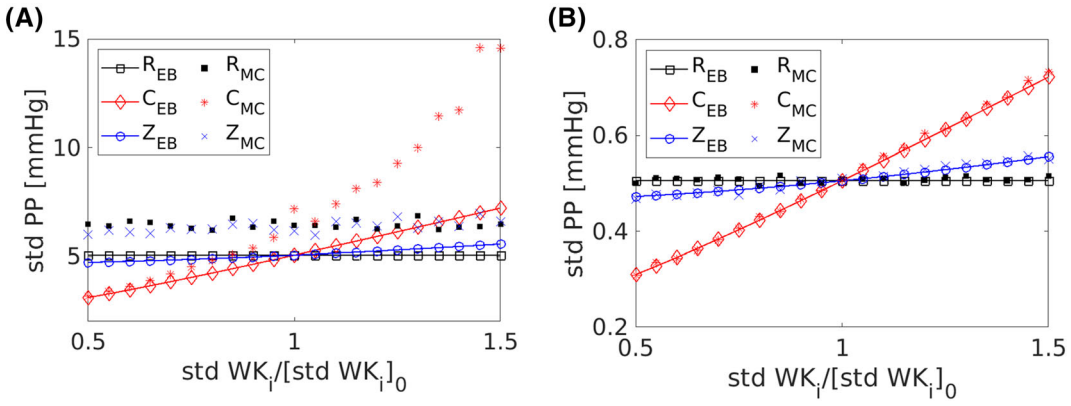

FIGURE 5 Pulse pressure uncertainty (STD PP) as a function of the standard deviations a Windkessel parameters ($WK_i = (R,C,Z)$) normalized by (A) the reference values shown in the first row of Table 1 and (B) 10% of the reference values, that is, $[stdR]_0 = 0.01622\frac{\text{mmHg}\cdot\text{s}}{\text{mL}}$, $[stdC]_0 = 0.03472\frac{\text{mL}}{\text{mmHg}}$ and $[stdC]_0 = 0.00073\text{mmHg}\frac{\text{mmHg}\cdot\text{s}}{\text{mL}}$. Expansion-based method results (EB) are represented by lines with dots and those obtained with Monte Carlo (MC) simulations with dots.

Our method requires a priori knowledge of the covariance matrix for the Windkessel and cardiac parameters, and the evaluation of the derivatives of the pressure against the Windkessel and cardiac parameters. Compared to other methodologies, like Monte Carlo simulations, our method is efficient since it avoids evaluating the governing equations many times, reducing the computation time by about 1/30. It is worth noting that estimating the pressure uncertainties using the Monte Carlo simulations is laborious, thus making it inefficient for practical applications. To measure the complexity and exhaustiveness of the Monte Carlo simulations compared to the proposed methodology, one should note that the former requires 15,000 times running the forward problem to solve for the pressure pulse wave (taking about half a minute per simulation, giving a total of 8 min to reproduce Figure 1). In contrast, the proposed method only needs a single simulation to predict the pressure signal (taking less than a second per simulation and a few seconds to reproduce Figure 1).

The expansion-based method can robustly propagate uncertainties due to the Windkessel parameters. Nonetheless, the accuracy reduces when uncertainties steaming from the flow waveform are considered (Figure 1). As discussed regarding the findings of Figure 1, the proposed method like all other local expansion-based methods is more reliable for small variations of the Windkessel parameters. Yet, it is worth noting concerning this figure that the predictions of the proposed formulation overestimate the uncertainties, which puts our estimations on the safe side when it is used for real-practice applications like wearable devices. In other words, the linear assumption incorporated in the proposed scheme gives rise to higher bounds of pressure uncertainty that puts the patients at a lower risk of mismanagement.

To illustrate how uncertainties of flow waveform propagate to the pressure, we used an uncertain flow waveform derived from variations of the SV and HR. When we only propagated the uncertainty due to the flow waveform (second row of Figure 1), the expansion-based method was not able to reproduce uncertainties in diastole. This is because in Equation (6), all the derivatives are equal to zero in diastole and, hence, the STD. Nonetheless, due to the relation between the mean flow and pressure ($\overline{P} = R_T/\overline{Q} + P_{\text{out}}$), a variation in the SV must change the mean pressure, which Monte Carlo simulations captured but not the expansion-base method. Uncertain flow waveforms are frequently encountered in clinical practice due to natural wave variations during each cardiac cycle. One way to remove such variations is to average measurements over a specific number of heart cycles obtaining a deterministic (averaged) single waveform. Nonetheless, uncertainties at each time point are presented. If one knows the uncertainties at each temporal point due to natural wave variations, our method could be applied to assess pressure uncertainties. We found that the proposed methodology is efficient and reliable for cases where flow waveform variations are much smaller than those of the Windkessel parameters.

We illustrated the applicability of the proposed methodology with the information of data sets at different age decades. The data sets correspond to an available database of pressure and flow waveforms obtained with a 1D model.[42] We found that the expansion-based method estimates higher standard deviations for the SBP (first row of Figure 3D) and DBP (second row of Figure 3D) than the database (approximately by a factor of 1.8 and 2.4, respectively) due to the uncertainties inherent to the zero-dimensional (0D) modeling. Namely, for 1D and 0D models with comparable cardiovascular properties, the 0D model overestimates the SBP and underestimates the DBP,[14] leading to higher SBP and DBP standard deviations. Our findings indicate that the variations in systolic and diastolic pressures across different age groups are similar to those observed in both in vivo and in vitro database.

Another use of uncertainty propagation is to obtain information about the sensitivity of the function to the input variables. We analyze the sensitivity of the SBP and DBP to the Windkessel parameters by varying their standard deviation. Our results show that variation of the standard deviation of the peripheral resistance produces the most remarkable change in the standard deviations of the SBP and DBP (see Figure 4A,B); this implies that a slight change in the peripheral resistance may lead to a significant variation of the SBP and DBP. The last result can be explained as follows, the peripheral resistance and characteristic impedance are related to the average pressure (Equation 15); consequently, a change in their values will cause a pressure waveform with a different mean value and consequently with a different systolic and diastolic pressures. Due to the peripheral resistance being at least one order of magnitude higher than the characteristic impedance (so its standard deviation), the variation of R induces the most significant change in the SBP and DBP.

We extended our framework to assess the pulse pressure uncertainty and found that the expansion-based method captures the trends dictated by the Monte Carlo simulations, see Figure 5A,B. When variations of the STD of the Windkessel parameters are small, Monte Carlo simulations and the proposed method reproduce similar results (see Figure 5B). However, when variations are relatively high, the proposed methodology underestimates the pulse pressure

uncertainty (see Figure 5A); this is due to the approximations considered in Equation (21), where the product of the SBP and DBP neglects the non-linear terms. Our analysis also identified that the compliance of the arterial system contributes the most significant change in the uncertainty of PP.

Our methodology has limitations; when using two temporal points of the pressure waveform, as in the pulse pressure, the nonlinear terms of the Taylor series may play an important role, leading to a rough uncertainty evaluation. In addition, this kind of frameworks are only robust for cases of relatively small input variability and (relatively) linear models. Although the presented expansion-based method is developed for the Windkessel model, it is a tool that can easily be applied to any model described by an ODE to assess how the model parameter's uncertainties propagate to the state variables.

5 | CONCLUSION

Recognizing the inherent trade-off between accuracy and accessibility in medical devices, wearable technology has emerged as a critical tool in alleviating the demands on clinical settings by providing convenient monitoring options. However, the precision of these devices in cardiovascular health monitoring varies, thus understanding the uncertainty associated with the pressure waveform estimated using their sensor data is crucial. The uncertainty estimation is instrumental in ensuring the reliability of data captured by multi-modal wearable sensors, thereby enabling clinicians to make more informed decisions.

For example, a systolic PPG-based blood pressure estimation reported with a 30% uncertainty level is significantly more trustworthy than one with a 60% uncertainty, as the standard deviation of the systolic pressure is a key determinant of its reliability. Our research introduces a theoretical method designed to rigorously estimate the uncertainty of the measured pressure waveform and its related indices. This advancement holds substantial importance for the interpretation of pressure waveform data across various modalities, enhancing the value of wearable devices in health monitoring and clinical decision-making.

In summary, our study provides a comprehensive examination of the uncertainty quantification of blood pressure waveforms generated by the Windkessel model and flow waveform, which has important implications for improving cardiovascular risk assessment and healthcare. The proposed local gradient-based uncertainty quantification framework demonstrates high efficiency and practicality for implementation in a variety of mathematical model applications. Specifically, we elucidated the method for quantifying the uncertainty of the pressure waveform resulting from the Windkessel parameters and showed the applicability of the formulation to assess systolic and diastolic blood pressure uncertainties.

The assumption of normally distributed parameters in the Windkessel model can have implications for uncertainty quantification and prediction accuracy. If this assumption no longer holds, it can challenge the validity of traditional statistical methods employed for analysis. In such cases, alternative approaches should be considered. One possibility is to explore non-parametric methods that do not rely on specific distribution assumptions, allowing for more flexible modeling. Additionally, techniques like bootstrapping or Bayesian inference can be employed to estimate the uncertainty in the absence of normality assumptions. However, given the estimative nature of the Windkessel model and the lack of clear information about the probability density function of the parameters, assuming a normal distribution is a sensible approach. Nonetheless, it is important to acknowledge the potential impact of departing from normality and consider alternative methodologies if the assumption no longer holds.

NOMENCLATURE

C	total arterial compliance
N	number of data points of the measured pressure signal
$\boldsymbol{P} = \mathbb{E}(\boldsymbol{P_m})$	expectation of measured pressure waveform (computed by the Windkessel model)
P_{out}	asymptotic (venous) pressure
R	peripheral resistance
$R_T = R + Z$	total arterial resistance
$\boldsymbol{X}$	parameters of the Windkessel model
Z	characteristic impedance
σ	standard deviation

SUBSCRIPTS

D diastolic pressure
PP pulse pressure
S systolic pressure

ACKNOWLEDGMENTS

The funding support for the postdoctoral fellowship from the Hong Kong Polytechnic University (project no. 1-YY4Y) is appreciated. The Hong Kong Center for Cerebro-Cardiovascular Health Engineering (COCHE) and InnoHK are also acknowledged.

DATA AVAILABILITY STATEMENT

The data that support the findings of this study are available from the corresponding author upon reasonable request.

ORCID

Joaquín Flores-Gerónimo https://orcid.org/0000-0002-8425-4520

REFERENCES

1. Westerhof N, Lankhaar JW, Westerhof BE. The arterial Windkessel. *Med Biol Eng Comput*. 2009;47:131-141. doi:10.1007/s11517-008-0359-2
2. Alastruey J, Charlton PH, Bikia V, et al. Arterial pulse wave modeling and analysis for vascular-age studies: a review from VascAgeNet. *Am J Physiol Heart Circ Physiol*. 2023;325(1):H1-H29. doi:10.1152/ajpheart.00705.2022
3. Westerhof N, Stergiopulos N, Noble MIM, Westerhof BE. *Snapshots of Hemodynamics: an Aid for Clinical Research and Graduate Education*. 3rd ed. Springer; 2019:207-215.
4. van de Vosse FN, Stergiopulos N. Pulse wave propagation in the arterial tree. *Annu Rev Fluid Mech*. 2011;43:467-499. doi:10.1146/annurev-fluid-122109-160730
5. Mariscal-Harana J, Charlton PH, Vennin S, et al. Estimating central blood pressure from aortic flow: development and assessment of algorithms. *Am J Physiol Heart Circ Physiol*. 2021;320(2):H494-H510. doi:10.1152/ajpheart.00241.2020
6. Olufsen MS, Peskin CS, Kim WY, Pedersen EM. Numerical simulation and experimental validation of blood flow in arteries with structured-tree outflow conditions. *Ann Biomed Eng*. 2000;28:1281-1299. doi:10.1114/1.1326031
7. Diaz-Ramirez LG, Lee SJ, Smith AK, Gan S, Boscardin WJ. A novel method for identifying a parsimonious and accurate predictive model for multiple clinical outcomes. *Comput Methods Prog Biomed*. 2021;204:106073. doi:10.1016/j.cmpb.2021.106073
8. Jansen JR, Wesseling KH, Settels JJ, Schreuder JJ. Continuous cardiac output monitoring by pulse contour during cardiac surgery. *Eur Heart J*. 1990;11(Suppl I):26-32. doi:10.1093/eurheartj/11.suppl_i.26
9. Wu BJ, Wu BF, Hsu CP. Camera-based blood pressure estimation via Windkessel model and waveform features. *IEEE Trans Instrum Meas*. 2022;72:1-13. doi:10.1109/TIM.2022.3224534
10. Oberkampf WL, DeLand SM, Rutherford BM, Diegert KV, Alvin KF. Error and uncertainty in modeling and simulation. *Reliab Eng Syst Saf*. 2002;75(3):333-357. doi:10.1016/S0951-8320(01)00120-X
11. Schäfer F, Sturdy J, Mesek M, et al. Uncertainty quantification and sensitivity analysis during the development and validation of numerical artery models. In: Nord LO, Komulainen T, Netzer C, Mirlekar G, Dongmo-Engeland B, Eriksson L, eds. *Proceedings of the 63rd International Conference of Scandinavian Simulation Society. Trondheim, Norway, September 20–21*. Scandinavian Simulation Society; 2022.
12. Marx L, Gsell MAF, Rund A, et al. Personalization of electro-mechanical models of the pressure-overloaded left ventricle: fitting of Windkessel-type afterload models. *Philos Trans R Soc A*. 2020;378:20190342. doi:10.1098/rsta.2019.0342
13. Gill RW. Measurement of blood flow by ultrasound: accuracy and sources of error. *Ultrasound Med Biol*. 1985;11(4):625-641. doi:10.1016/0301-5629(85)90035-3
14. Epstein S, Willemet M, Chowienczyk PJ, Alastruey J. Reducing the number of parameters in 1D arterial blood flow modeling: less is more for patient-specific simulations. *Am J Physiol Heart Circ Physiol*. 2015;309:H222-H234. doi:10.1152/ajpheart.00857.2014
15. Chen P, Quarteroni A, Rozza G. Simulation-based uncertainty quantification of human arterial network hemodynamics. *Int J Numer Meth Biomed Eng*. 2013;29:698-721. doi:10.1002/cnm.2554
16. Quicken S, Donders WP, van Disseldorp EM, et al. Application of an adaptive polynomial chaos expansion on computationally expensive three-dimensional cardiovascular models for uncertainty quantification and sensitivity analysis. *J Biomech Eng*. 2016;138(12):4034709. doi:10.1115/1.4034709
17. Lee S, Rajan S, Dajani HR, Groza VZ, Bolic M. Determination of blood pressure using Bayesian approach. *IEEE International Instrumentation and Measurement Technology Conference*. IEEE; 2011:1-5. doi:10.1109/IMTC.2011.5944338
18. Turner MJ, Irwig L, Bune AJ, Kam PC, Baker AB. Lack of sphygmomanometer calibration causes over- and under-detection of hypertension: a computer simulation study. *J Hypertens*. 2006;24(10):1931-1938. doi:10.1097/01.hjh.0000244940.11675.82
19. Xiu D, Sherwin SJ. Parametric uncertainty analysis of pulse wave propagation in a model of a human arterial network. *J Comput Phys*. 2007;226(2):1385-1407. doi:10.1016/j.jcp.2007.05.020

20. Kolh P, D'Orio V, Lambermont B, Gerard P, Gommes C, Limet R. Increased aortic compliance maintains left ventricular performance at lower energetic cost. *Eur J Cardiothorac Surg*. 2000;17:272-278. doi:10.1016/S1010-7940(00)00341-9
21. Geven MC, Bohte VN, Aarnoudse WH, et al. A physiologically representative in vitro model of the coronary circulation. *Physiol Meas*. 2004;25:891-904. doi:10.1088/0967-3334/25/4/009
22. Mol A, Rutten MCM, Driessen NJB, et al. Autologous human tissue-engineered heart valves: prospects for systemic application. *Circulation*. 2006;114:I152-I158. doi:10.1161/CIRCULATIONAHA.105.001123
23. Zhou S, Xu L, Hao L, et al. A review on low-dimensional physics-based models of systemic arteries: application to estimation of central aortic pressure. *Biomed Eng Online*. 2019;18(41):41. doi:10.1186/s12938-019-0660-3
24. Dewi EM, Hadiyoso S, Mengko TLER, Zakaria H, Astami K. Cardiovascular system modeling using Windkessel segmentation model based on Photoplethysmography measurements of fingers and toes. *J Med Signals Sens*. 2022;12(3):192-201. doi:10.4103/jmss.jmss_101_21
25. Huppert TJ, Allen MS, Benav H, Jones PB, Boas DA. A multicompartment vascular model for inferring baseline and functional changes in cerebral oxygen metabolism and arterial dilation. *J Cereb Blood Flow Metab*. 2007;27(6):1262-1279. doi:10.1038/sj.jcbfm.9600435
26. Antonuccio MN, Mariotti A, Fanni BM, et al. Effects of uncertainty of outlet boundary conditions in a patient-specific case of aortic coarctation. *Ann Biomed Eng*. 2021;49(12):3494-3507. doi:10.1007/s10439-021-02841-9
27. Fevola E, Bradde T, Triverio P, Grivet-Talocia S. A vector fitting approach for the automated estimation of lumped boundary conditions of 1D circulation models. *Cardiovasc Eng Technol*. 2023;14:505-525. doi:10.1007/s13239-023-00669-z
28. Fanni BM, Antonuccio MN, Pizzuto A, Berti S, Santoro G, Celi S. Uncertainty quantification in the in vivo image-based estimation of local elastic properties of vascular walls. *J Cardiovasc Dev Dis*. 2023;10(3):109. doi:10.3390/jcdd10030109
29. Tricarico R, Berceli SA, He Y. Non-invasive estimation of the parameters of a three-element windkessel model of aortic arch arteries in patients undergoing thoracic endovascular aortic repair. *Front Bioeng Biotechnol*. 2023;11:1127855. doi:10.3389/fbioe.2023.1127855
30. Nair PJ, Pfaller MR, Dual SA, McElhinney DB, Ennis DB, Marsden AL. Non-invasive estimation of pressure drop across aortic coarctations: validation of 0D and 3D computational models with in vivo measurements. *medRxiv* 2023.09.05.23295066. 2023. doi:10.1101/2023.09.05.23295066
31. Yu H, Khan M, Wu H, et al. Inlet and outlet boundary conditions and uncertainty quantification in volumetric lattice Boltzmann method for image-based computational hemodynamics. *Fluids*. 2022;7(1):30. doi:10.3390/fluids7010030
32. Yuhn C, Oshima M, Chen Y, Hayakawa M, Yamada S. Uncertainty quantification in cerebral circulation simulations focusing on the collateral flow: surrogate model approach with machine learning. *PLoS Comput Biol*. 2022;18(7):e1009996. doi:10.1371/journal.pcbi.1009996
33. Aristizábal-Ocampo D, Álvarez-Montoya D, Madrid-Muñoz C, Fallon-Giraldo S, Gallo-Villegas J. Hemodynamic profiles of arterial hypertension with ambulatory blood pressure monitoring. *Hypertens Res*. 2023;46:1482-1492. doi:10.1038/s41440-023-01196-z
34. Odeigah OO, Wall ST, Sundnes J. Computational models of ventricular mechanics and adaptation in response to right-ventricular pressure overload. *Front Physiol*. 2022;13:936. doi:10.3389/fphys.2022.948936
35. He Y, Northrup H, Le H, Cheung AK, Berceli SA, Shiu YT. Medical image-based computational fluid dynamics and fluid-structure interaction analysis in vascular diseases. *Front Bioeng Biotechnol*. 2022;10:855791. doi:10.3389/fbioe.2022.855791
36. Guzzetti S, Mansilla Alvarez LA, Blanco PJ, Carlberg KT, Veneziani A. Propagating uncertainties in large-scale hemodynamics models via network uncertainty quantification and reduced-order modeling. *Comput Methods Appl Mech Eng*. 2020;358:112626. doi:10.1016/j.cma.2019.112626
37. Paun LM, Colebank MJ, Olufsen MS, Hill NA, Husmeier D. Assessing model mismatch and model selection in a Bayesian uncertainty quantification analysis of a fluid-dynamics model of pulmonary blood circulation. *J R Soc Interface*. 2020;17(173):20200886. doi:10.1098/rsif.2020.0886
38. Fanni BM, Gasparotti E, Vignali E, Capelli C, Positano V, Celi S. An integrated in-vitro and in-silico workflow to study the pulmonary bifurcation hemodynamics. *Comput Fluids*. 2023;260:105912. doi:10.1016/j.compfluid.2023.105912
39. Salvador M, Regazzoni F, Dede' L, Quarteroni A. Fast and robust parameter estimation with uncertainty quantification for the cardiac function. *Comput Methods Prog Biomed*. 2023;231:107402. doi:10.1016/j.cmpb.2023.107402
40. Santiago A, Butakoff C, Eguzkitza B, et al. Design and execution of a verification, validation, and uncertainty quantification plan for a numerical model of left ventricular flow after LVAD implantation. *PLoS Comput Biol*. 2022;18(6):e1010141. doi:10.1371/journal.pcbi.1010141
41. Gray RA, Pathmanathan P. Patient-specific cardiovascular computational modeling: diversity of personalization and challenges. *J Cardiovasc Transl Res*. 2018;11(2):80-88. doi:10.1007/s12265-018-9792-2
42. Charlton PH, Mariscal HJ, Vennin S, Li Y, Chowienczyk P, Alastruey J. Modeling arterial pulse waves in healthy aging: a database for in silico evaluation of hemodynamics and pulse wave indexes. *Am J Physiol Heart Circ Physiol*. 2019;317(5):H1062-H1085. doi:10.1152/ajpheart.00218.2019
43. Straley A, Hampton TG, Soto PF, Ower CH, Davis JW, Glower DD. Arterial Windkessel parameter estimation: a new time-domain method. *Ann Biomed Eng*. 1994;22(6):66-77. doi:10.1007/BF02368223
44. Geffray C, Gerschenfeld A, Kudinov P, et al. Verification and validation and uncertainty quantification. In: Roelofs F, ed. *Thermal Hydraulics Aspects of Liquid Metal Cooled Nuclear Reactors*. Woodhead Publishing; 2019:383-405. doi:10.1016/B978-0-08-101980-1.00008-9
45. Sin G, Gernaey KV, Lantz AE. Good modeling practice for PAT applications: propagation of input uncertainty and sensitivity analysis. *Biotechnol Prog*. 2009;25:1043-1053. doi:10.1002/btpr.166
46. Coleman HW, Steele WG. *Experimentation, Validation, and Uncertainty Analysis for Engineers*. 3rd ed. John Wiley & Sons, Inc; 2009.

47. Rouaud M. Probability, statistics and estimation. *Propagation of Uncertainties in Experimental Measurement*. Creative Commons; 2013.
48. Stergiopulos N, Westerhof BE, Westerhof N. Total arterial inertance as the fourth element of the Windkessel model. *Am J Physiol Heart Circ Physiol*. 1999;276(1):H81-H88. doi:10.1152/ajpheart.1999.276.1.H81
49. Kind T, Faes TJC, Lankhaar JW, Vonk-Noordegraaf A, Verhaegen M. Estimation of three- and four-element Windkessel parameters using subspace model identification. *IEEE Trans Biomed Eng*. 2010;57(7):1531-1538. doi:10.1109/TBME.2010.2041351
50. Braun M. *Differential Equations and their Applications: an Introduction to Applied Mathematics*. 4th ed. Springer; 1993.
51. Dart AM, Kingwell BA. Pulse pressure -a review of mechanisms and clinical relevance. *J Am Coll Cardiol*. 2001;37(4):975-984. doi:10.1016/s0735-1097(01)01108-1
52. McEniery CM, Yasmin HIR, Qasem A, Wilkinson IB, Cockcroft JR, Investigators ACCT. Normal vascular aging: differential effects on wave reflection and aortic pulse wave velocity: the Anglo-Cardiff collaborative trial (ACCT). *J Am Coll Cardiol*. 2005;46:1753-1760. doi:10.1016/j.jacc.2005.07.037

How to cite this article: Flores-Gerónimo J, Keramat A, Alastruey J, Zhang Y. Uncertainty quantification of the pressure waveform using a Windkessel model. *Int J Numer Meth Biomed Engng*. 2024;40(12):e3867. doi:10.1002/cnm.3867

APPENDIX A

The uncertainty steaming from each data set in Table 1 was propagated in the pressure waveform to illustrate the applicability of the expansion-based method. Figure A1 shows the aortic pressure waveform and their uncertainties from decades 35 to 65 years old.

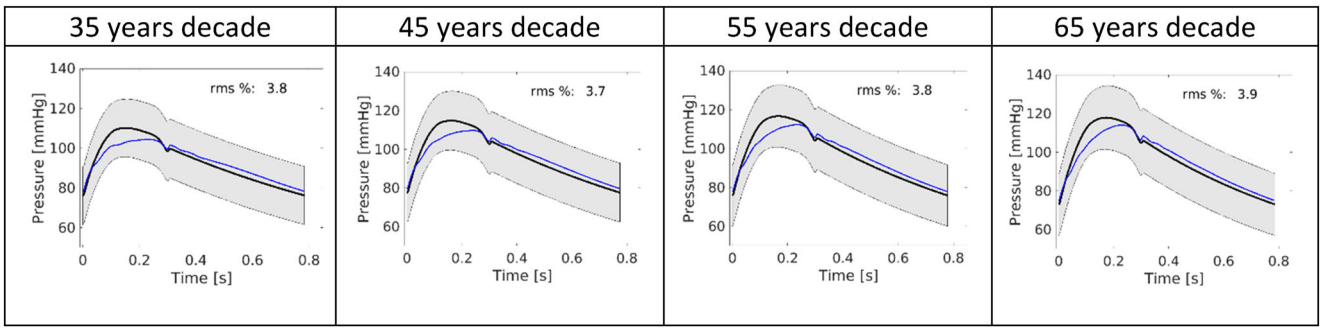

FIGURE A1 Aortic pressure with standard deviations; from 35 to 65 decades. The shaded area shows the standard deviation of pressure obtained with Equation (6). The black line is the pressure for the mean values of the Windkessel parameters. The blue line is the aortic pressure from the base subject of the decade.[42] The root mean square error with the baseline subject's pressure as a reference is shown in each plot.